Numerically Efficient Miniaturization-Oriented Optimization of an Ultra-Wideband Spline-Parameterized Antenna

ADRIAN BEKASIEWICZ[1], (Senior Member, IEEE), **PIOTR KURGAN**[1], (Member, IEEE),
AND SLAWOMIR KOZIEL[1,2], (Fellow, IEEE)

[1]Faculty of Electronics, Telecommunications and Informatics, Gdańsk University of Technology, 80-233 Gdańsk, Poland
[2]Department of Engineering, Reykjavik University, 101 Reykjavik, Iceland

Corresponding author: Adrian Bekasiewicz (bekasiewicz@ru.is)

ABSTRACT Design of ultra-wideband radiators for modern handheld applications is a challenging task that involves not only selection of an appropriate topology, but also its tuning oriented towards balancing the electrical performance and size. In this work, a low-cost design of a compact, broadband, spline-parameterized monopole antenna has been considered. The framework used for the structure design implements trust-region-based methods, space mapping correction mechanisms, and a meta-optimization loop that permits a gradual increase of the problem dimensionality. The optimized structure is characterized by small dimensions of 11.4 mm × 17.2 mm and an overall footprint of only 195 mm^2. The radiator operates within 3.1 GHz to 12 GHz bandwidth with the reflection coefficient amplitude level of around –10 dB. The computational cost of the structure design amounts to just 163 simulations of the high-fidelity EM model, which is low having in mind that the antenna is represented by a total of 38 adjustable parameters. The optimized radiator has been compared against state-of-the-art structures from the literature. Benchmarking of the presented optimization algorithm has also been performed. Numerical results have been confirmed by measurements of the fabricated antenna prototype.

INDEX TERMS Antenna miniaturization, computer-aided design, meta-optimization, spline-based antennas, surrogate-based optimization, trust-region methods, UWB antennas.

I. INTRODUCTION

After years of development, ultra-wideband (UWB) technology makes its way to modern handheld and wearable devices as a hardware layer for precise localization and identification in Internet of Things (IoT) applications. Small size and high performance belong to the most important prerequisites for implementation of UWB antennas in modern devices. The main problem with miniaturization of these structures is that physical dimensions bound from below the wavelength traveling in the wireless medium that can be coupled to the radiator [1], [2]. Conventional size-reduction techniques boil down to implementation of antennas on relatively expensive high-permittivity substrates [3], [4]. Alternatively, small

The associate editor coordinating the review of this manuscript and approving it for publication was Derek Abbott.

footprints can be achieved using unconventional antenna topologies [5], [6].

The development of compact radiators for UWB communication (here understood as a frequency range from 3.1 GHz to 10.6 GHz) is the topic of ongoing research [5]–[14]. Dominant size reduction approaches discussed in the literature are oriented towards modifications of conventional antenna topologies such as planar monopoles or dipoles using suitable geometry features [7]–[10]. Popular techniques involve introduction of various slots [13], [15], [16], and/or stubs [14], [15], [17]. Other realizations are oriented towards development of self-complementary geometries [18], [19], protruded ground planes [20], [21], impedance transformers [16], [17], or meandered structures [13], [15]. Application of the mentioned geometry modifications allows for reducing radiators dimensions even

A. Bekasiewicz *et al.*: Numerically Efficient Miniaturization-Oriented Optimization of UWB Spline-Parameterized Antenna

IEEE *Access*

below 400 mm^2 [13], [15], [16], [20], [22]. For example, in [13], an antenna characterized by a footprint of only 175 mm^2 has been obtained through introduction of a meandered stepped slot into the ground plane. Another topology, proposed in [15], implements a combination of a meandered *L*-shaped ground plane stub and a rectangular slot to maintain acceptable electrical performance for a small size of 348 mm^2. Due to complex geometry, accurate evaluation of the discussed structures can be performed only by means of expensive full-wave electromagnetic (EM) simulations.

Regardless of the substantial differences between the discussed compact antenna topologies, they share a common, cognitive design approach [23], which boils down to the determination of the basic geometry followed by its modifications in hope for improved performance while maintaining acceptable size of the radiator [14], [20], [24]. Although the introduction of miniaturization-oriented geometry changes should be followed by parametric analysis of the antenna performance, or (preferably) its numerical optimization, these steps are often neglected due to a corresponding high computational cost. The outcome of the discussed manual or semi-manual design approaches is the structure tuned with respect to a selected performance figure (typically in-band reflection coefficient amplitude). Its remaining properties, such as size or field characteristics are just by-products of the experience-driven design process. Consequently, a number of small antennas from the literature are at best sub-optimal in terms of both size and performance [25]. The consequence of such a state of the matter is not only the lack of reliable means for qualitative comparison of various antenna topologies but also larger dimensions of the obtained radiators compared to the ones that would result from a rigorous numerical optimization [25]. Finally, bias of the designer resulting from the experience in dealing with selected classes of antenna modifications narrows down the number of topology choices being verified in the course of a compact structure development.

The mentioned challenges can be mitigated by means of systematic, optimization-based approaches to the generation and tuning of antenna topologies. Automatic topology generation can be achieved through representation of the radiator in the form of a binary matrix where zeros and ones correspond to the metal-less (etched) and metal sections of the structure [26], [27]. Alternatively, the antenna can be implemented as a set of characteristic points interconnected using line sections or curves [28], [29]. Optimization-based adjustment of point location allows for changing structure topology w.r.t. the imposed performance specifications. Conventional approaches to the discussed evolution-based design of antennas rely on utilization of population-based optimization algorithms [30], [31]. However, due to a high computational cost associated with hundreds to thousands of antenna model evaluations required for algorithm convergence, topology generation techniques are often limited to rather simple structures with a small number of input parameters. To put that into perspective, in [30], a particle-swarm-based optimization of the radiator

represented using only five dimensions required 4200 EM simulations to converge, whereas in [32] a total of 2100 evaluations was required to find the acceptable solution for a design represented using four points. The problem with low-dimensional structures is that they are of limited use for miniaturization due to insufficient flexibility in terms of a trade-off between size and performance. This is one of the main reasons for which small-form-factor structures obtained using manual design approaches are often characterized by over a dozen of input parameters [14]–[16]. From this perspective the availability of the methods for generation of multi-parameter (hence, flexible in terms of the specification) structures at an acceptable computational cost is of high importance.

The challenges related to the high cost of the topology generation can be addressed using surrogate-based optimization (SBO) [33]–[38]. The goal of SBO is to shift the computational burden of the optimization from the expensive high-fidelity EM antenna model to a numerically cheap surrogate. The latter is constructed from the inaccurate low-fidelity simulations enhanced using an appropriate correction layer [33]. A surrogate-assisted design involves an iterative approximation of the desired solution through optimization of the structure in a prediction-correction loop [37]. The prediction step—realized through optimization of the surrogate model—generates a new approximation of the design, whereas the correction involves update of the surrogate based on the obtained high-fidelity data. Space mapping (SM) represents a popular class of model correction methods used for low-cost antenna design. Its most successful implementations in antenna design include variants of output- and frequency-based corrections [33], [38]. Other approaches such as adaptive response correction, or manifold mapping also proved to be useful for simulation-driven design of radiators [39]. Application of surrogate-assisted design methods is considered important for maintaining an acceptable cost of the automated design of compact antennas.

In this work, a numerically efficient design of a compact, planar UWB monopole antenna represented using a set of spline-connected characteristic points is considered. The low cost of the radiator design has been ensured using a surrogate-assisted framework that integrates space mapping correction mechanisms and a gradient-based trust-region algorithm, both embedded in a meta-optimization loop which gradually increases the number of parameters used for the structure representation. The considered antenna has been optimized using a composite objective function which balances the trade-off between miniaturization and the required reflection coefficient amplitude (here, around –10 dB within 3.1 GHz to 10.6 GHz frequency band). The presented design optimization scheme has been benchmarked in terms of the computational cost and performance with alternative TR-based algorithms. The optimized radiator is characterized by a footprint of only 195 mm^2. The structure has been compared against the state-of-the-art compact monopoles from

the literature. The numerical results have been confirmed by measurements of the fabricated antenna prototype.

II. ANTENNA STRUCTURE

Consider a planar monopole antenna shown in Fig. 1. The structure is implemented on a Rogers RO4003C dielectric material (ε_r = 3.38, h = 0.813 mm, $\tan\delta$ = 0.0027). It is composed of a radiator fed through a microstrip line and the ground plane with an L-shaped extension [17], [40]. The latter increases electrical size of the structure and hence promotes obtaining small size while maintaining acceptable electrical performance. The radiator and ground plane are represented using a set of points interconnected using spline curves. The set of antenna design parameters is $y = [y_a \ y_g \ y_r]^T$. The vector $y_a = [X \ l_f \ l_1 \ l_{2r} \ w_1 \ o_r]^T$ represents "static" dimensions of the structure, whereas $y_g = [y_{g.1} \ldots y_{g.L}]^T$ and $y_r = [y_{r.1} \ldots y_{r.L}]^T$, $L = 50$, are the coordinates of points that constitute the radiator and ground plane, respectively (cf. Fig. 1). The relative variables used in the antenna model are $l_2 = (X - w_1)l_{2r}$, $Y = l_1 + w_1$, $l_{fr} = \min\{0.5X, 0.5(Y - l_f)\}$, $o = 0.5X + o_r$. The width of the antenna feed is fixed to $w_f = 1.8$ which corresponds to a 50-Ohm input impedance. All parameters are in mm except l_{2r} which is dimensionless. For the sake of geometrical consistency, the driven element and the ground plane are defined with respect to the antenna external dimensions as $y_g = Y \cdot z_g$, and $y_r = S \cdot z_r$, where $S = \min\{0.5(X - o_r), 0.5(Y - l_f)\}$ (note that the antenna size is $A = S \cdot Y$). Furthermore, the characteristic points from y_g and y_r sets are evenly spaced. This allows to address possible challenges related to their overlap resulting in unwanted intersection of the generated curves. It should be noted that, for the radiator, even distance between points has been obtained through their representation in a cylindrical coordinate system.

The high-fidelity model of the antenna structure comprises (on average) ∼400 000 hexahedral mesh cells. Its typical evaluation time on a dual Xeon E5-2650 machine with 64 GB RAM is 162 seconds. The low-fidelity model consists of about 30 000 mesh cells and its simulation time is 37 seconds. Besides relaxed mesh settings, other simplifications introduced to the low-fidelity model include representation of metal layers in the form of a perfect electrical conductor and a reduced computational domain. Both structures are implemented in CST Microwave Studio and evaluated using its time-domain solver [41]. It is worth noting that a total of $2L$ points used for parameterization of the antenna ground plane and radiator have been generated using an appropriate macro [41].

Owing to the curve-based representation of the EM models, the number of points used for antenna optimization can be adjusted in the course of the design process. In other words, in the given meta-iteration the optimizer can be configured to represent splines using a pre-defined number of points. Consequently, at the beginning of the design process the antenna can be represented using a small number of parameters. Upon identification of the promising region

the dimensionality can be gradually increased to exploit the search space and improve antenna performance. An analogy to this approach might be observation of the Earth from a high altitude (low number of variables) where only the largest features can be identified on the ground (which is similar to the functional landscape). With decreasing altitude (growing number of input parameters), one gains more detailed insight into a particular (narrowed down) region. Here, the antenna dimensionality can be adjusted through implicit handling of adjustable parameters. Let $x_d = [y_a \ x_{g.d} \ x_{r.d}]^T$, where $x_{g.d} = [x_{g.1} \ldots x_{g.d}]^T$, $x_{r.d} = [x_{r.1} \ldots x_{r.d}]^T$, $d = 1, \ldots, L$, be the vectors representing the ground plane and radiator using d control points. Modification of the dimensionality of the structure is implemented through interpolation of $x_{g.d}$ and $x_{r.d}$ to $z_g = z_{g.L}$ and $z_r = z_{r.L}$ vectors (note that L corresponds to the number of points used for the representation of antenna EM models features). The process can be defined as follows:

$$z_{\{g,r\}} \leftarrow \text{ip} \left(x_{\{g,r\}.d}, L \right) \tag{1}$$

where ip is the function that interpolates d-dimensional input parameter vector to the L-point one. The conversion process is transparent to the EM models and the optimization routine. The lower and upper bounds for the structure design are $l_b = [6 \ 4 \ 10 \ 0.05 \ 0.5 \ -1 \ l_{g.d} \ l_{r.d}]^T$ and $u_b = [30 \ 15 \ 30 \ 1 \ 2.5 \ 1 \ u_{g.d} \ u_{r.d}]^T$, where $l_{g.d} = [0.2 \ldots 0.2]^T$, $l_{r.d} = [0.1 \ldots 0.1]^T$, and $u_{g.d} = [0.8 \ldots 0.8]^T$, $l_{r.d} = [1 \ldots 1]^T$. Hence, $x_{g.d}$, $x_{r.d} \in [0.1 \ 0.8]$.

III. DESIGN METHODOLOGY

This section is devoted to the description of the design methodology. In particular, we formulate the optimization problem, but also discuss the low-fidelity model correction mechanisms, as well as the optimization engine used for structure design. The discussion is followed by the explanation of the meta-optimization scheme and a summary of the design framework. Numerical results concerning optimization of the antenna structure are provided in Section IV.
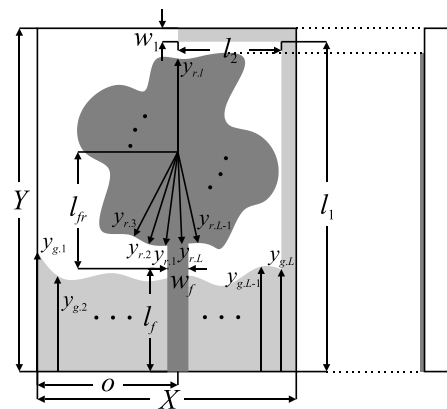

FIGURE 1. Conceptual illustration of the spline-parameterized monopole antenna with highlighted design variables. Dark and light grey represent top and bottom metallization, respectively.

A. PROBLEM DEFINITION

Let $R_f(x_d)$ and $R_c(x_d)$ represent the high- and the low-fidelity models of the antenna at hand obtained for the x_d vector of adjustable parameters, where d in subscript denotes the number of control points used for representation of the spline-parameterized antenna geometry. The design problem regarding optimization of the structure can be defined as a nonlinear minimization task of the following form [38]:

$$x_d^* = \arg \min_{x_d} U(R_f(x_d)) \qquad (2)$$

where U is a scalar objective function and x_d^* is the optimal design to be found. The computational cost of (2) is often numerically prohibitive as it requires a large number of high-fidelity EM model simulations to converge [33], [38]. In order to mitigate this problem, direct optimization can be replaced by an iterative process of the form [35]:

$$x_d^{(i+1)} = \arg \min_{x_d} U(R_s^{(i)}(x_d)) \qquad (3)$$

The goal of (3) is to shift the computational burden associated with R_f model optimization to a cheap surrogate $R_s^{(i)}$, which is constructed from the R_c model, enhanced by using an underlying correction layer. In other words, the process (3) generates a series of approximations ($i = 1, 2, \ldots$) to the original problem through optimizations of the surrogate in a prediction-correction loop [37]. The prediction step is geared towards approximating the desired solution, which is then validated using the high-fidelity simulations [33]. The high-fidelity data is also used to update the surrogate model so as to allow for further exploitation of the search space oriented towards narrowing down the design subspace containing the desired solution [33].

B. LOW-FIDELITY MODEL CORRECTION

The correction layer for the low-fidelity model is based on the space mapping methodology [33]. Here, a combination of the implicit SM and frequency scaling is used. The surrogate model is defined as:

$$R_s(x_d) = R_s(x_d, p, \alpha) = R_c(x_d, p, \alpha) \qquad (4)$$

Here, the vector p represents a set of so-called preassigned parameters that are associated with properties of the substrate material (thickness, permittivity, or loss tangent) used for implementing the antenna [42]. Their modification affects electrical behavior of the low-fidelity model, and hence its responses. Consequently, the vector p can be adjusted so as to match the surrogate to the high-fidelity model characteristics (at the given design $x_d^{(i)}$). The parameter set $\alpha = [\alpha_1 \alpha_2]^T$ represents coefficients used for scaling of the structure responses. Let $f = [f_1 f_2 \ldots f_Q]^T$ represent the Q-point frequency sweep for which the low-fidelity antenna reflection has been evaluated (i.e., $R_c(x_d) = R_c(x_d, f)$). The goal of frequency scaling is to alter the original characteristics through replacement of the original sweep with $\omega = \alpha_1 + f\alpha_2$. Substitution of f with ω in the R_s model allows the stretching or squeezing as well as shifting of its frequency

response with respect to high-fidelity simulations. The values of correction coefficients p, α are obtained in the course of a separate optimization task—a so-called parameter extraction (PE) [33]. The latter is defined as a minimization problem of the following form:

$$[p, \alpha] = \arg \min_{p, \alpha} \left(\left\| R_f \left(x_d^{(i)} \right) - R_s(x_d^{(i)}, p, \alpha) \right\| \right) \qquad (5)$$

The process (5) realizes a curve-fitting of the surrogate model responses to the high-fidelity data at the given design $x_d^{(i)}$. It should be noted that concurrent optimization of both sets of correction parameters is performed. Although the computational cost of frequency scaling is negligible (it is performed through interpolation of readily available low-fidelity model responses), adjustment of preassigned parameters involves modifications of the model properties followed by its evaluation which makes them computationally expensive when EM-based simulations are used in the PE process [43]. To address this problem, direct solving of (5) is replaced by an iterative procedure embedded in a trust-region (TR) framework. The details concerning TR-based optimization engine are provided in the following section. For more elaborated discussion on the applications of space mapping for the low-fidelity model correction, see [33], [39].

C. OPTIMIZATION ENGINE

The optimization engine used in this work for the implementation of the prediction-correction mechanism discussed in Section III. A is a gradient algorithm embedded in a modified trust-region (TR) framework [43], [44]. The method generates a series of approximations j = 1, 2, ..., to the problem at hand. The generic formulation of the TR routine is given as [44]:

$$s^{(j+1)} = \arg \min_{s: \|s - s^{(j)}\| \leq r^{(j)}} U\left(G^{(j)}(s) \right) \qquad (6)$$

where s is the vector of parameters under optimization (here, $s = x_d$ or $s = \beta = [p, \alpha]^T$; depending on the operation mode of the algorithm) and $G^{(j)}$ is a local Taylor-expansion model of the following form:

$$G^{(j)}(s) = R\left(s^{(j)} \right) + J\left(s^{(j)} \right) \left(s - s^{(j)} \right) \qquad (7)$$

Here, $R(s) = R_f(x_d)$ for the predictive part of the design process and $R(s) = R_s(\beta) = R_s(x_d^{(i)}, p, \alpha)$ when the optimization oriented for PE is considered. The Jacobian $J(s^{(j)})$ is generated around the nominal design $s^{(j)}$ using a large-step finite differentiation [44], i.e.,

$$J\left(s^{(j)} \right) = \begin{bmatrix} \left(R_s \left(s^{(j)} + g_1 \right) - R_s \left(s^{(j)} \right) \right) / g_1 \\ \vdots \\ \left(R_s \left(s^{(j)} + g_m \right) - R_s \left(s^{(j)} \right) \right) / g_m \\ \vdots \\ \left(R_s \left(s^{(j)} + g_M \right) - R_s \left(s^{(j)} \right) \right) / g_M \end{bmatrix}^T \qquad (8)$$

The vector $g_m = [0 \ldots g_m \ldots 0]^T$, whereas g_m is the perturbation size w.r.t. mth dimension ($M = 2d + |y_a|$ is the

dimensionality of the considered design problem, where $|y_a|$ denotes cardinality of the y_a vector; cf. Section II).

The trust-region radius $r^{(j)}$, i.e., determining the region for which the linear model (7) is considered valid, is controlled based on a gain ratio which expresses predicted versus obtained improvement of the objective function response [44]:

$$\rho = \frac{U\left(R\left(s^{(j+1)}\right)\right) - U\left(R\left(s^{(j)}\right)\right)}{U\left(G^{(j)}\left(s^{(j+1)}\right)\right) - U\left(G^{(j)}\left(s^{(j)}\right)\right)} \quad (9)$$

The algorithm (6) is terminated when one (or more) of the following holds:

$$r^{(j+1)} \leq \varepsilon$$
$$\left\| s^{(j+1)} - s^{(j)} \right\|_2 \leq \varepsilon$$
$$j \geq j_{\max} \quad (10)$$

where ε and $j_{\max}$ are the user-specified values. The former (here, $\varepsilon = 10^{-2}$) represents acceptable threshold of the TR radius/Euclidean distance between consecutive designs. Parameter $j_{\max}$ denotes the maximum allowed number of algorithm iterations.

As already mentioned, the algorithm (6) is used for two design tasks: (i) parameter extraction and (ii) surrogate model optimization. During the PE step, the Jacobian $G_{PE}^{(j)}(s^{(j)}) = G^{(j)}(\beta^{(j)})$ is generated only once in order to reduce the computational burden of the process. Consequently, for successful iterations only the center design $R(s^{(j)}) = R_s(\beta^{(j)}) = R_s(x_d^{(i)}, \beta^{(j)})$ is updated in (7)—note that design parameters $x_d^{(i)}$ do not take part in the PE process. Furthermore, the maximum number of TR iterations for PE is limited to $j_{\max} = 5$. The initial TR radius is set to $r^{(0)} = 1$ and is updated as follows. When $\rho > 0.75$, $r^{(j+1)} = 2r^{(j)}$, whereas for $\rho < 0.25$, $r^{(j+1)} = 0.25 \cdot \|\beta^{(j+1)} - \beta^{(j)}\|$. The objective function U_{PE} is defined as a least-squares problem of the form:

$$U_{PE}(\beta) = U_{PE}(p, \alpha) = U_{PE}(p, \alpha_1 + f\alpha_2)$$
$$= \frac{1}{Q} \sum_{q=1}^{Q} \left(R_f\left(x_d^{(i)}, f_q\right) - G_{PE}^{(j)}\left(x_d^{(i)}, p, \alpha_1 + f_q\alpha_2\right) \right)^2 \quad (11)$$

It is worth noting that the computational cost of the PE step is low as it amounts only to a few low-fidelity model simulations required for construction of the Jacobian and only one R_s simulation per successful/unsuccessful iteration.

For the surrogate model optimization, the algorithm setup is slightly different compared to the one discussed above. First of all, the model correction mechanisms of Section III. B do not ensure zero-order consistency (i.e., a perfect match between the surrogate and high-fidelity model responses), which is required for a reliable algorithm operation [44]. To address this problem, the algorithm uses surrogate model responses only for the construction of the Jacobian, whereas the response at the center design $x_d^{(j)}$ is obtained based on the high-fidelity model simulations. It should be emphasized

that the R_f model data have to be obtained in each TR step in order to calculate the gain ratio. Therefore, "blending" of the R_s and R_f model responses in (7) does not affect the computational cost of the algorithm.

The optimizer permits updating the Jacobian only when failed design (i.e., $\rho < 0$) is obtained after one (or a series) of successful steps ($\rho > 0$). Finally, when re-generation of the Jacobian does not produce an improved solution, the TR radius is decreased as $r^{(j+1)} = r^{(j)}/3$. The initial radius is set to $r^{(0)} = 1/\max(d - 2, 1)$. The consequence of the introduced modifications is that the derivative data obtained around jth design can be reused for a range of successful iterations which reduces the optimization cost w.r.t. conventional implementations of the TR routine. As a result, the cost of the method operation (excluding the PE step) amounts to a single R_f simulation for each iteration, as well as M R_c simulations in the first iteration and each unsuccessful step after a series of the ones that improved the objective function response.

The optimization engine can be summarized as follows:

1. Set $j = 0$, $j_{\mathrm{tmp}} = j$, $x_d^{(0)}$, $\beta^{(0)}$ and mode $= 2$;
2. Generate Jacobian around $\beta^{(0)}$ and construct the local approximation model $G_{PE}^{(j)}$ (with $x_d = x_d^{(j\mathrm{tmp})}$);
3. Find $\beta^{(j+1)}$ through minimization of (11) using (6);
4. Evaluate $R_s(\beta^{(j+1)})$, $R_s(\beta^{(j)})$, $G_{PE}^{(j)}(\beta^{(j+1)})$, and $G_{PE}^{(j)}(\beta^{(j)})$ and calculate ρ;
5. If $\rho > 0.75$, set $r^{(j+1)} = 2r^{(j)}$; If $\rho < 0.25$, set $r^{(j+1)} = 0.25 \cdot \|\beta^{(j+1)} - \beta^{(j)}\|$;
6. If $\rho > 0$ update (7) using $R_s(\beta^{(j+1)})$; otherwise set $\beta^{(j+1)} = \beta^{(j)}$;
7. If the termination condition is met set $\beta = \beta^{(j+1)}$, $j = 0$ and go to Step 8; otherwise, set $j = j + 1$ and go to Step 3;
8. Set $j = j_{\mathrm{tmp}}$;
9. Generate the Jacobian around $x_d^{(j)}$ using the surrogate model responses (with β obtained from Step 7) and construct the local model using $R_f(x_d^{(j)})$ in (7);
10. Find $x_d^{(j+1)}$ through optimization of the objective function U (cf. Section III. D);
11. Evaluate $R_f(x_d^{(j+1)})$, $R_f(x_d^{(j)})$, $G^{(j)}(x_d^{(j+1)})$, and $G^{(j)}(x_d^{(j)})$ and calculate ρ;
12. If $\rho > 0.75$, set $r^{(j+1)} = 2r^{(j)}$; If $\rho < 0.25$ and mode $= 2$, set $r^{(j+1)} = r^{(j)}/3$; If $\rho < 0.25$ and mode $= 0$, set mode $= 1$;
13. If $\rho > 0$ set mode $= 0$ and go to Step 14; otherwise go to Step 16;
14. Update (7) using $R_f(x_d^{(j+1)})$, set $j = j + 1$;
15. If the termination condition is met, END; otherwise go to Step 10;
16. If $\rho < 0$ and mode $= 1$, set $j_{\mathrm{tmp}} = j$, $\beta^{(0)} = \beta$, $j = 0$, mode $= 2$, and go to Step 2.

In the proposed algorithm, the first seven steps are dedicated to the PE process, whereas the remaining ones realize optimization of the surrogate model. As can be noticed, the regeneration of the Jacobian for the stage concerning antenna optimization can be activated only when the algorithm

A. Bekasiewicz *et al.*: Numerically Efficient Miniaturization-Oriented Optimization of UWB Spline-Parameterized Antenna

IEEE *Access*

operation mode is set to 1 and the gain ratio is below zero. The presented TR-based optimization routine noticeably reduces the number of low-fidelity model simulations compared to more conventional algorithms where the derivative data is re-generated after each successful iteration. As a consequence, the method is useful for handling design problems characterized by a large number of input parameters.

D. OBJECTIVE FUNCTION

The objective function used in the optimization process is designed to achieve an acceptable balance between the size reduction and electrical performance of the antenna of Section II. It takes different forms depending on the stage of the optimization process, aiming at (i) an unconstrained reduction of the in-band reflection coefficient amplitude, (ii) miniaturization with a performance-related constraint, and (iii) a size-constrained minimization of the reflection coefficient amplitude. The objective function for the first stage is of the following form:

$$U_1(\boldsymbol{x}_d) = \max(|S_{11}| - S_{\max.1}) \qquad (12)$$

Here, $|S_{11}| = \boldsymbol{R}(\boldsymbol{x}_d)_{fL \leq f \leq fH}$—evaluated based on the high-fidelity or surrogate model responses—is the antenna reflection coefficient amplitude over a frequency range specified by the lower and upper corner frequencies f_L and f_H ($f_L, f_H \in \boldsymbol{f}$). The parameter $S_{\max.1} = -10$ dB is the user-defined, lower-level threshold of the electrical performance. The objective function (12) is used for the structure design until the obtained objective function value is lower than zero. Then the optimization process is handled by using:

$$U_2(\boldsymbol{x}_d) = A(\boldsymbol{x}_d) + \gamma_1 \max(U_1(\boldsymbol{x}_d)/|S_{\max.1}|, 0)^2 \quad (13)$$

The antenna size $A(\boldsymbol{x}_d)$ is defined in Section II, whereas γ_1 is a user-defined scaling factor that controls the contribution of the penalty component to the objective function (13). Here, $\gamma_1 = 1000$ so as to ensure noticeable values of the additive term for a relatively small violation of the threshold concerning the acceptable reflection coefficient amplitude. The function (13) remains active until the requirement $\max(|S_{11}|) \leq S_{\max.2}$ holds (here, $S_{\max.2} = -9.5$ dB is the upper-level performance threshold). Otherwise the optimization procedure is handed over to:

$$U_3(\boldsymbol{x}_d) = \max(|S_{11}|) + \gamma_2 \max\left(\left(A(\boldsymbol{x}_d) - A_{\max}^{(o)}\right)/A_{\max}^{(o)}, 0\right)^2 \qquad (14)$$

where $A_{\max}^{(o)}$, $o = 1, \ldots, O$, is the antenna footprint obtained before switching from (13) to (14), whereas the coefficient $\gamma_2 = 500$. The function U_3 is active when $\max(|S_{11}|) \geq S_{\max.1}$. Otherwise the optimization is again transferred to U_2. The algorithm for controlling the composite objective function can be summarized as follows:

1. Set $S_{\max.1}, S_{\max.2}, \gamma_1, \gamma_2, o = 1$;
2. Optimize antenna through minimization of (12) using algorithm of Section III. *C*;

3. If $\max(|S_{11}|) \leq S_{\max.1}$ go to Step 4; otherwise go to Step 2;
4. Minimize (13) using algorithm of Section III. *C*;
5. If $\max(|S_{11}|) \geq S_{\max.2}$ set $A_{\max}^{(o)} = A(\boldsymbol{x}_d)$, $o = o+1$; and go to Step 6; otherwise go to Step 4;
6. Minimize (14) using algorithm of Section III. *C*;
7. If $\max(|S_{11}|) \leq S_{\max.1}$ go to Step 4; otherwise go to Step 6.

In summary, the proposed algorithm first optimizes the electrical performance of the antenna and then switches the optimization task between two objective functions in order to seeks for a balance between the antenna size and its in-band reflection coefficient amplitude. It should be noted that the termination of the algorithm of Section III. *C* is triggered when the objective function value cannot be further improved. Due to the selected $S_{\max.1}$ and $S_{\max.2}$ thresholds, the optimized design might slightly violate the requirement concerning the desired -10 dB reflection coefficient amplitude level. A conceptual illustration of the optimization process using the proposed composite function is shown in Fig. 2.
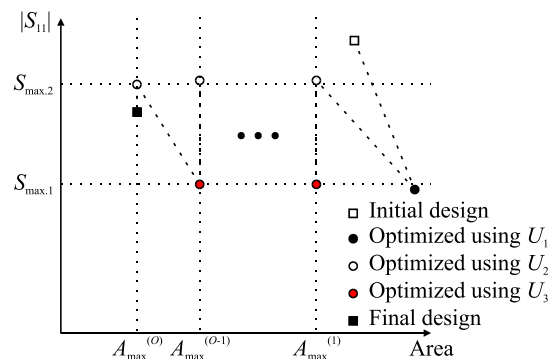

FIGURE 2. Conceptual illustration of the antenna performance and size changes in the course of the optimization using a composite objective function. Note that $A_{\max}^{(1)}$ to $A_{\max}^{(O)}$ refer to $A(\boldsymbol{x}_d^{(j)})$ values obtained during switching between the U_2 and U_3 objective functions.

E. META-OPTIMIZATION AND SUMMARY OF THE DESIGN FRAMEWORK

The surrogate-assisted optimization algorithm of Section III. *C* is embedded in a meta-optimization loop which gradually increases the number of design parameters used for representation of spline curves that constitute the antenna at hand. As already mentioned, the sequential increase of problem dimensionality allows for the more in-depth exploitation of the search space region already narrowed down by optimizing the low-dimensional structure representation.

Let $\boldsymbol{d} = [d_1 \ldots d_n]^T$, $n = 1, \ldots, N$, be a set of n positive integer values that define the number of spline parameters used to represent the antenna radiator/ground plane. Also, let $\boldsymbol{x}_d = \boldsymbol{x}_{dn}$ (note that $d = d_n$) denote the vector of structure parameters represented using d_n spline variables (note that $d_n \in [1, L]$; cf. Section II). In each meta-iteration n, the design $\boldsymbol{x}_{dn}^*$ obtained by the TR algorithm is used as a starting

point for the next step. In other words, the design $x_{dn+1}^{(0)}$ is obtained through interpolation of x_{dn}^* using d_{n+1} spline points as in (1) and then optimized using method of Section III. *C*. The design process is terminated either when the number of meta-iterations is equal to N or when increasing the number of design parameters for consecutive iterations does not improve objective function value.

The design framework embedded in a meta-optimization loop can be summarized as follows:

1. Define d, set $n = 1$, and $x_{d1}^{(0)}$;
2. Obtain x_{dn}^* using algorithm of Section III. *C*;
3. If termination condition is met, END; otherwise, set $x_{dn+1}^{(0)} \leftarrow \text{ip}(x_{dn}^*, d_{n+1})$, $n = n + 1$ and go to Step 2.

It should be noted that the size of the vector d substantially affects the computational cost of design optimization. The reason is that each meta-iteration is in fact a separate TR optimization. On the other hand, gradual increase of problem dimensionality allows mitigating the risk of the TR algorithm getting stuck in a poor minimum. The latter is a serious challenge when local optimization of multi-dimensional design problems (as in the case of this work) is considered.

IV. NUMERICAL RESULTS AND DISCUSSION

The antenna structure of Section II has been optimized using a design framework of Section III. The vector representing the number of spline parameters for the consecutive meta-iterations has been set to $d = [1\ 8\ 16\ 24\ 32]^T$ (hence, $N = 5$). The preassigned variables for the PE have been set to $p = [h\ \varepsilon_r\ \tan\delta]^T$. In order to keep the PE cost low, the low-fidelity model substrate has not been divided into segments [43]. Consequently the total number of parameters for PE amounts to just five. The frequency range of interest is from $f_L = 3.1$ GHz to $f_H = 10.6$ GHz which covers the entire UWB spectrum.

The initial design is $x_1^{(0)} = [10\ 6\ 16\ 0.8\ 1\ 0\ 0.35\ 0.6]^T$. In the first meta-step, the solution $x_1^* = [12.14\ 4.57\ 16.1\ 0.81\ 2.08\ -0.31\ 0.37\ 0.56]^T$ has been found after 12 iterations of the algorithm of Section III. *C*. The resulting structure is characterized by the in-band reflection coefficient amplitude of -6.4 dB which violates the $S_{\max,1}$ threshold. Next, the design x_1^* has been interpolated to $x_8^{(0)}$ as explained in Section III. *E*. The solution $x_8^* = [11.39\ 4.77\ 15.58\ 0.91\ 1.62\ -0.19\ 0.44\ 0.46\ 0.27\ 0.2\ 0.4\ 0.45\ 0.25\ 0.2\ 0.67\ 0.5\ 0.53\ 0.45\ 0.84\ 0.73\ 0.61\ 0.61]^T$ has been found after 31 iterations of the TR algorithm. The resulting structure is characterized by a footprint of 195.9 mm² and the in-band reflection coefficient amplitude below the -9.6 dB level. The design has been used as a starting point for the next stage, where the following set of adjustable variables has been obtained after 14 iterations $x_{16}^* = [11.37\ 4.77\ 15.56\ 0.91\ 1.61\ -0.19\ 0.44\ 0.5\ 0.47\ 0.39\ 0.31\ 0.21\ 0.19\ 0.24\ 0.35\ 0.43\ 0.47\ 0.43\ 0.34\ 0.23\ 0.17\ 0.2\ 0.67\ 0.52\ 0.5\ 0.53\ 0.54\ 0.48\ 0.43\ 0.53\ 0.76\ 0.87\ 0.81\ 0.7\ 0.64\ 0.61\ 0.6\ 0.61]^T$. The optimized structure is characterized by the in-band reflection coefficient amplitude of -9.8 dB,

with dimensions of 11.37 mm × 17.17 mm and an overall footprint of only 195.2 mm². It should be noted that the third meta-iteration not only improved the in-band reflection coefficient amplitude of the antenna but also slightly reduced its footprint. However, the achieved performance improvement is relatively small. Due to the lack of objective function improvement, the optimization has been terminated after the fourth meta-step ($d_4 = 24$). The convergence plots of the optimization algorithm obtained for each meta-iteration are shown in Fig. 3. It should be noted that steady increase of the distance between the consecutive designs for $n = 2$ ($d_2 = 8$) in the middle of the optimization results from switching between the design objectives as described in Section III. *D*.

A comparison of matching characteristics obtained for the antenna designs optimized in consecutive meta-iterations is shown in Fig. 4. Visualizations of the antenna geometries at $x_1^{(0)}$ and at the end of each design stage are shown in Fig. 5. It should be noted that, although the initial design is noticeably smaller than the final one (170 mm² vs. 195 mm²), it is also characterized by an unacceptable in-band reflection coefficient amplitude of -3.4 dB. Conversely, the optimized antenna exhibits a decent performance (in-band matching below or equal to -9.6 dB), while being only 15 percent larger in comparison to the starting point. It is worth noting that the matching characteristics at x_8^* and x_{16}^* are almost the same.

At first the degradation of the objective function response at the transition from x_{16}^* to x_{24}^* might be counterintuitive. However, it is caused by the "noise" induced by the approximation of spline curves represented by using d_n points and an increased d_{n+1} dimensional data set. The consequence is an imperfect reconstruction of the structure shape at the transition between the two structure representations, which results in a slight worsening of the performance. At some point in the design process (here, for $n = 4$), the latter cannot be corrected because a local curvature of the functional landscape becomes "saturated" and a further increase of problem dimensionality does not lead to meaningful changes of its shape.

The realized gain and total efficiency characteristics obtained for the x_{16}^* design are shown in Fig. 6. The average in-band gain in the x-direction (cf. Fig. 5) and in the angle of maximum propagation are 0.61 dB and 3.6 dB, respectively. The discrepancies between the responses result from small dimensions of the structure and relatively wide *L*-shaped strip which acts as a reflector. Another cause of the misalignment is a slight angular instability of the gain with the frequency. The problem could be potentially addressed through introduction to the objective function a component dedicated to maintaining control over the gain stability. However, it exceeds the scope of the work. The average total efficiency of the structure within the band of interest is 92% which is acceptable (especially having in mind small dimensions of the antenna). It should be noted that a local degradation of efficiency around 8 GHz and 10 GHz frequencies coincides with the maxima of the in-band reflection coefficient (cf. Fig. 4).
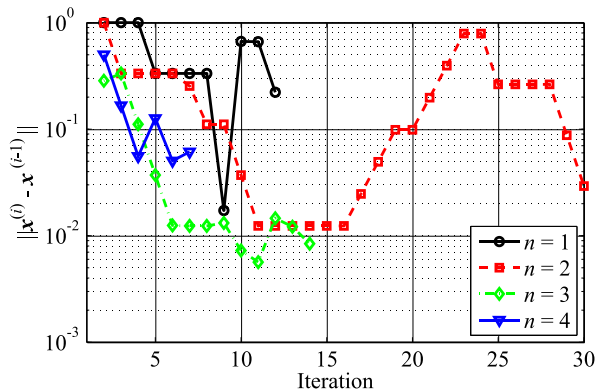
A. Bekasiewicz *et al.*: Numerically Efficient Miniaturization-Oriented Optimization of UWB Spline-Parameterized Antenna

IEEE *Access*

FIGURE 3. Numerical optimization: convergence plots obtained for meta-iterations n = 1, 2, 3, 4.
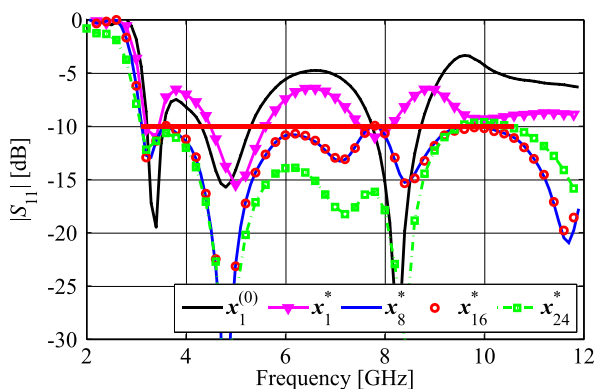

FIGURE 4. Comparison of the spline-parameterized antenna characteristics at the initial design (black) and the optimized designs obtained in each meta-iteration. Red horizontal line denotes the desired level of in-band matching.

FIGURE 5. In-scale visualization of the spline-parameterized antenna designs. From the left-hand side: $x_1^{(0)}$ (area: 170 mm^2), x_1^* (area: 220.6 mm^2), x_8^* (area: 195.9 mm^2), and x_{16}^* (area: 195.2 mm^2).
Note that the difference between the x_8^* and x_{16}^* is minor.

FIGURE 6. Responses of the optimized antenna design x_{16}^*: (a) realized gain in the angle of maximum propagation (blue) and x-direction (red; cf. Fig. 5), as well as (b) total efficiency.

The computational cost of structure optimization using the proposed algorithm corresponds to 163.3 high-fidelity model evaluations (~7.4 hours of CPU-time), which is low having in mind that the antenna is represented using up to 54 independent parameters. The design cost includes a total of 448 R_c model simulations required for PE and the construction of the Jacobians, as well as 61 R_f model evaluations performed for validation of the responses. The proposed algorithm has been benchmarked against alternative design approaches that include: (i) TR method embedded in the meta-optimization framework that exploits only R_f model simulations, as well as two techniques oriented towards optimization of designs represented by 38 variables (n = 3), i.e., (ii) direct TR using only R_f model responses, and (iii) design using the algorithm of Section III. *C*. Furthermore, in (iv), the antenna has been optimized only using (13) to justify the usefulness of the proposed combined objective function (cf. Section III. *D*). The numerical results gathered in Table 1 indicate that the proposed optimization routine outperforms the benchmark algorithms. The computational cost of the presented approach is 73% and 54% lower in comparison to (i) and (ii), respectively. It should be emphasized that, due to the local search nature of the TR routine the method (iii) was incapable of finding acceptable design solutions. Finally, the algorithm (iv) also
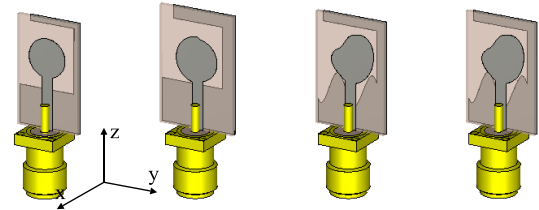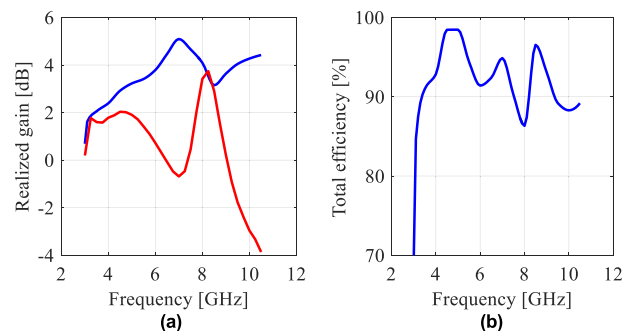
produced the design solution that violates the performance requirements. It is worth noting that, although the cost of third meta-iteration performed using the presented algorithm is noticeable, it does not result in a substantial performance improvement. Consequently, an adjustment of the proposed routine for further reduction of the computational cost might be considered in the future.

The optimized antenna design x_{16}^* has been compared against the state-of-the-art monopoles from the literature in terms of the size and bandwidth (expressed as a ratio of high-to-low corner frequencies) [15], [18], [24], [45]–[47]. For the sake of fair comparison, the dimensions of antennas are expressed w.r.t. the guided wavelength λ_g (calculated for the lower corner frequency f_L defined at the –10 dB level and electrical parameters of the substrate used for the implementation of the structure at hand). The results gathered in Table 2 indicate that the optimized radiator offers the smallest dimensions among the compared structures while maintaining competitive performance. It is worth noting that the presented antenna is around 40% and up to 60% smaller than the structures featuring similar and broader bandwidth, respectively. The mentioned properties make the proposed antenna potentially useful for mobile devices that implement services based on Internet of Things technology [22], [48].

V. MEASUREMENTS
The optimized antenna structure (design x_{16}^*) has been fabricated and measured. Photographs of the manufactured

IEEE *Access*

A. Bekasiewicz *et al.*: Numerically Efficient Miniaturization-Oriented Optimization of UWB Spline-Parameterized Antenna

prototype are shown in Fig. 7. A comparison of the reflection responses and realized gain (in x-direction) over frequency obtained from simulations and measurements is provided in Fig. 8. The discrepancy between the obtained in-band matching maxima (Fig. 8(a)) is around 1 dB. At the same time, the fabricated structure is characterized by a slightly right-shifted lower operational frequency (to 3.185 GHz form the intended 3.1 GHz). For the gain response (Fig. 8(b)), the misalignment between the simulations and measurements over the frequency of interest amounts to around 0.9 dB. At the same time, average measured gain is 0.35 dB, just slightly lower compared to the one obtained from EM simulations (0.61 dB). Note that the peak gain measurements (cf. Fig. 6(a)) are not provided due to limitations of our gear.

It is worth emphasizing that shape-related difference between the characteristics from Fig. 8(a) results from distortions of the radiator performance caused by current flow on the outer shell of the measurement cables. This phenomena is calibration independent and noticeably affects electrical size of the small antenna [49], [50]. In this work, the effect has been accounted for (to some extent) by means of post-processing. The structure response has been measured in a time domain and modified using a window function. The reflection shown in Fig. 8(a) has been obtained through conversion of the window-corrected time-domain signal to the frequency spectrum [51], [52]. For more information on the approach see [49]–[52].

The comparisons of antenna co- and cross-polar radiation patterns obtained from simulations and measurements in the x-y plane (cf. Fig. 5) at 4 GHz, 7 GHz, 8 GHz, and 10 GHz frequencies are shown in Fig. 9. The obtained results indicate that, for lower frequencies, the co-polar component of the response is dominant. However, the contribution of the cross-polar pattern increases with frequency and peaks around the 8 GHz. The increased effect of the cross-polar component is also manifested by the visible gain spike around 8 GHz frequency (see. Fig. 8(b)). Such behavior results from asymmetrical geometry of the radiator. It is worth noting that, for the considered spline antenna, the balance between horizontal (cross-polar) and vertical (co-polar) radiation patterns can be maintained through controlling topology of the structure using appropriately defined objective function. This concept, however, exceeds the scope of the work and will be considered elsewhere.

It should be emphasized that the measured field characteristics have been obtained in a non-anechoic environment using the time-gating method [53], [54]. Having in mind non-ideal measurement conditions, the agreement between simulations and measurements in terms of both electrical and field performance figures is acceptable.

The main contributors to the discrepancies between the responses (in terms of electrical- and field-related characteristics) include fabrication tolerances, manual assembly of the antenna prototype (connector preparation, positioning, and soldering), and setup used for the structure measurements

TABLE 1. Spline antenna: design cost using benchmark algorithms.

Method	n	R_c (opt)	R_c (PE)	R_c (Σ)	R_c [R_f]	R_f	Total [R_f]	Total [h]
(i)	1	–	–	–	–	76	76	3.42
	2	–	–	–	–	491	491	22.10
	3	–	–	–	–	39	39	1.76
	Σ	–	–	–	–	606	606	27.28
(ii)	–	–	–	–	–	356	356	16.02
(iii)*	–	190	41	231	52.8	17	69.8	3.14
(iv)*	–	–	–	–	–	241	241	10.85
This work	1	24	27	51	11.6	11	22.6	1.02
	2	154	46	200	45.7	31	76.7	3.45
	3	114	22	136	31.1	13	44.1	1.98
	4	54	7	61	13.9	6	19.9	0.90
	Σ	346	102	448	102.3	61	163.3	7.35

* The final design substantially violates the electrical specifications

TABLE 2. Comparison of the optimized structure with the state-of-the-art antennas.

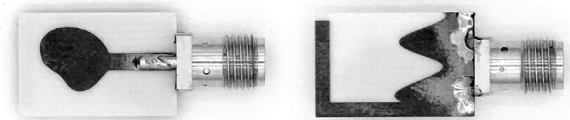| Structure	f_L [GHz]	Bandwidth	Dimensions [mm × mm]	Size [mm²]	Dimensions [$\lambda_g \times \lambda_g$]	Size [λ_g^2]
[45]	2.9	3.3:1	32.0 × 36.0	1152	0.56 × 0.64	0.359
[46]	4.0	10:1	28.1 × 17.1	481	0.68 × 0.42	0.285
[47]	2.9	7.7:1	25.0 × 17.0	425	0.44 × 0.30	0.132
[24]	3.1	4.5:1	14.5 × 22.0	319	0.28 × 0.43	0.120
[8]	3.0	3.6:1	10.0 × 32.5	325	0.18 × 0.59	0.106
[15]	3.1	3.4:1	15.8 × 22.0	348	0.22 × 0.31	0.070
This work	3.1	3.9:1	11.4 × 17.2	195	0.19 × 0.29	0.056

FIGURE 7. Spline-parameterized monopole antenna – photograph of the fabricated structure prototype: top (left) and bottom (right).
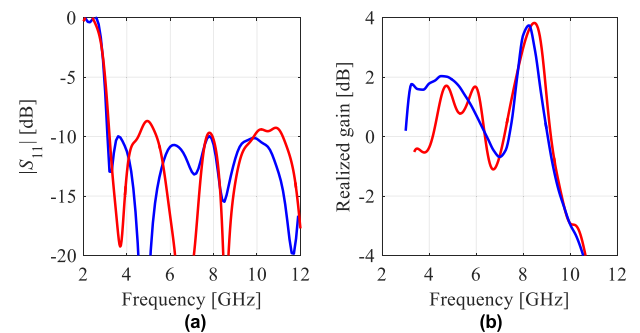

FIGURE 8. A comparison of antenna responses obtained from simulations (blue) and measurements (red): (a) reflection coefficient and (b) realized gain in x-direction (see Fig. 5).

(non-anechoic environment, or the effects of coaxial cables on electrical size of the compact radiator [49]). Furthermore,
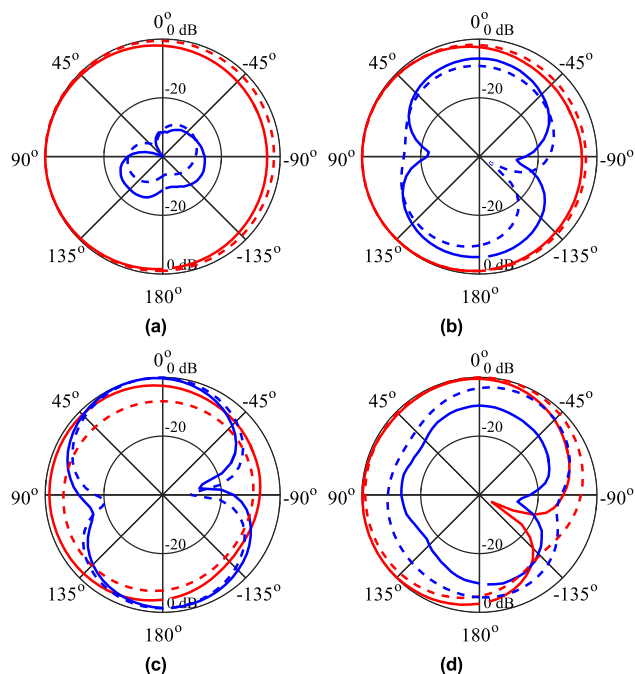
A. Bekasiewicz *et al.*: Numerically Efficient Miniaturization-Oriented Optimization of UWB Spline-Parameterized Antenna

IEEE *Access*

FIGURE 9. A comparison of the normalized co- (red) and cross-polar (blue) E-field radiation patterns obtained in the x-y plane (cf. Fig. 5) through simulations (dashed lines) and measurements (solid lines) at: (a) 4 GHz, (b) 7 GHz, (c) 8 GHz, and (d) 10 GHz.

the radiation pattern errors are affected by misalignment of the planes between the reference and the tested antenna.

VI. CONCLUSION

A low-cost design optimization of a compact spline-parameterized UWB antenna has been presented. The proposed design framework implements space-mapping-based correction of the low-fidelity model responses, modified TR-based algorithm capable of handling design optimization and extraction of SM parameters, as well as meta-iteration loop which gradually increases the number of design parameters used for representation of the antenna geometry. The unconventional radiator, optimized using the proposed routine, is characterized by small dimensions of 11.4 mm × 17.2 mm and an overall footprint of only 195 mm^2. Furthermore, the structure operates within 3.1 GHz to 12 GHz bandwidth which makes it of a potential use for the pulse-based localization and/or other Internet of Things applications. The presented design algorithm has been validated against conventional TR-based optimization methods. The results indicate that the cost of the method is up to around 70% lower w.r.t. to benchmark algorithms. Furthermore, the structure has been favorably compared with ultra-wideband antennas from the literature in terms of size and electrical performance. Numerical results have been confirmed by measurements of the fabricated prototype.

Future work will focus on implementing the concept of meta-iterations to design of microwave and antenna structures in a genuine multi-objective setup. The development

of method oriented towards adjustment of the increase of step size (parameter-wise) between meta-iterations so as to mitigate the problem of shape-approximation-related noise will also be considered. Furthermore, the objective function enhancement through combination of the electrical performance characteristics with the field-related ones (e.g., axial ratio, or gain) while maintaining main focus around the antenna size reduction will be investigated.

REFERENCES

[1] J. Volakis, C.-C. Chen, and K. Fujimoto, *Small Antennas: Miniaturization Techniques and Applications*. New York, NY, USA: McGraw-Hill, 2010.

[2] S. Dey and N. C. Karmakar, "Design of novel super wide band antenna close to the fundamental dimension limit theory," *Sci. Rep.*, vol. 10, Oct. 2020, Art. no. 16306.

[3] A. S. Alqadami, N. Nguyen-Trong, B. Mohammed, A. E. Stancombe, M. T. Heitzmann, and A. Abbosh, "Compact unidirectional conformal antenna based on flexible high-permittivity custom-made substrate for wearable wideband electromagnetic head imaging system," *IEEE Trans. Antennas Propag.*, vol. 68, no. 1, pp. 183–194, Sep. 2019.

[4] A. A. Baba, R. M. Hashmi, K. P. Esselle, and A. R. Weily, "Compact high-gain antenna with simple all-dielectric partially reflecting surface," *IEEE Trans. Antennas Propag.*, vol. 66, no. 8, pp. 4343–4348, Aug. 2018.

[5] T. K. Roshna, U. Deepak, V. R. Sajitha, K. Vasudevan, and P. Mohanan, "A compact UWB MIMO antenna with reflector to enhance isolation," *IEEE Trans. Antennas Propag.*, vol. 63, no. 4, pp. 1873–1877, Apr. 2015.

[6] M. S. Khan, A.-D. Capobianco, S. M. Asif, D. E. Anagnostou, R. M. Shubair, and B. D. Braaten, "A compact CSRR-enabled UWB diversity antenna," *IEEE Antenna Wireless Propag. Lett.*, vol. 16, pp. 808–812, 2016.

[7] M. G. N. Alsath and M. Kanagasabai, "Compact UWB monopole antenna for automotive communications," *IEEE Trans. Antennas Propag.*, vol. 63, no. 9, pp. 4204–4208, Sep. 2015.

[8] Y.-F. Liu, P. Wang, and H. Qin, "Compact ACS-fed UWB monopole antenna with extra Bluetooth band," *Electron. Lett.*, vol. 50, no. 18, pp. 1263–1264, 2014.

[9] A. Dumoulin, M. John, M. J. Ammann, and P. McEvoy, "Optimized monopole and dipole antennas for UWB asset tag location systems," *IEEE Trans. Antennas Propag.*, vol. 60, no. 6, pp. 2896–2904, Jun. 2012.

[10] S. M. Nair, V. A. Shameena, R. Dinesh, and P. Mohanan, "Compact semicircular directive dipole antenna for UWB applications," *Electron. Lett.*, vol. 47, no. 23, pp. 1260–1262, Nov. 2011.

[11] W. S. Yeoh and W. S. T. Rowe, "An UWB conical monopole antenna for multiservice wireless applications," *IEEE Antennas Wireless Propag. Lett.*, vol. 14, pp. 1085–1088, 2015.

[12] J. Nan, J. Zhao, M. Gao, W. Yang, M. Wang, and H. Xie, "A compact 8-States frequency reconfigurable UWB antenna," *IEEE Access*, vol. 9, pp. 144257–144263, 2021.

[13] Q.-X. Chu, C.-X. Mao, and H. Zhu, "A compact notched band UWB slot antenna with sharp selectivity and controllable bandwidth," *IEEE Trans. Antennas Propag.*, vol. 61, no. 8, pp. 3961–3966, Aug. 2013.

[14] L. Liu, S. W. Cheung, and T. I. Yuk, "Compact MIMO Antenna for portable devices in UWB applications," *IEEE Trans. Antennas Propag.*, vol. 61, no. 8, pp. 4257–4264, Aug. 2013.

[15] A. Bekasiewicz and S. Koziel, "Structure and computationally-efficient simulation-driven design of compact UWB monopole antenna," *IEEE Ant. Wireless Prop. Lett.*, vol. 14, pp. 1282–1285, 2015.

[16] S. K. Palaniswamy, Y. Panneer, M. G. Alsath, M. Kanagasabai, S. Kingsly, and S. Subbaraj, "3D eight-port ultra-wideband (UWB) antenna array for diversity applications," *IEEE Ant. Wireless Prop. Lett.*, vol. 16, pp. 569–572, 2017.

[17] T. Li, H. Zhai, G. Li, L. Li, and C. Liang, "Compact UWB band-notched antenna design using interdigital capacitance loading loop resonator," *IEEE Antennas Wireless Propag. Lett.*, vol. 11, pp. 724–727, 2012.

[18] J. Zhu, S. Li, B. Feng, L. Deng, and S. Yin, "Compact dual-polarized UWB quasi-self-complementary MIMO/diversity antenna with band-rejection capability," *IEEE Antennas Wireless Propag. Lett.*, vol. 15, pp. 905–908, 2016.

[19] C.-Y. Huang and J.-Y. Su, "A printed band-notched UWB antenna using quasi-self-complementary structure," *IEEE Antennas Wireless Propag. Lett.*, vol. 10, pp. 1151–1153, 2011.

IEEE Access

A. Bekasiewicz *et al.*: Numerically Efficient Miniaturization-Oriented Optimization of UWB Spline-Parameterized Antenna

[20] J.-F. Li, Q.-X. Chu, Z.-H. Li, and X.-X. Xia, "Compact dual band-notched UWB MIMO antenna with high isolation," *IEEE Trans. Antennas Propag.*, vol. 61, no. 9, pp. 4759–4766, Sep. 2013.

[21] X. Qing and Z. N. Chen, "Compact coplanar waveguide-fed ultra-wideband monopole-like slot antenna," *IET Microw., Antennas Propag.*, vol. 3, no. 5, pp. 889–898, 2009.

[22] N. Chahat, M. Zhadobov, R. Sauleau, and K. Ito, "A compact UWB antenna for on-body applications," *IEEE Trans. Antennas Propag.*, vol. 59, no. 4, pp. 1123–1131, Apr. 2011.

[23] J. Mroczka, "The cognitive process in metrology," *Measurement*, vol. 46, no. 8, pp. 2896–2907, Oct. 2013.

[24] S. S. Al-Bawri, G. H. Hwang, M. S. Islam, H. Y. Wong, M. F. Jamlos, A. Narbudowicz, M. Jusoh, T. Sabapathy, R. Khan, and M. T. Islam, "Compact ultra-wideband monopole antenna loaded with metamaterial," *Sensors*, vol. 20, p. 796, Oct. 2020.

[25] S. Koziel and A. Bekasiewicz, "Comprehensive comparison of compact UWB antenna performance by means of multiobjective optimization," *IEEE Trans. Antennas Propag.*, vol. 65, no. 7, pp. 3427–3436, Jul. 2017.

[26] S. Mirhadi, N. Komjani, and M. Soleimani, "Ultra wideband antenna design using discrete Green's functions in conjunction with binary particle swarm optimization," *IET Microw., Antennas Propag.*, vol. 10, pp. 184–192, Oct. 2016.

[27] J. Alnas, G. Giddings, and N. Jeong, "Bandwidth improvement of an inverted-F antenna using dynamic hybrid binary particle swarm optimization," *Appl. Sci.*, vol. 11, Oct. 2021, Art. no. 2559.

[28] B. Dong, J. Yang, J. Dahlström, J. Flygare, M. Pantaleev, and B. Billade, "Optimization and realization of quadruple-ridge flared horn with new spline-defined profiles as a high-efficiency feed from 4.6 GHz to 24 GHz," *IEEE Trans. Antennas Propag.*, vol. 67, no. 1, pp. 585–590, Jan. 2019.

[29] M. Ghassemi, M. Bakr, and N. Sangary, "Antenna design exploiting adjoint sensitivity-based geometry evolution," *IET Microw., Antennas Propag.*, vol. 7, no. 4, pp. 268–276, 2013.

[30] L. Lizzi, F. Viani, R. Azaro, and A. Massa, "Optimization of a spline-shaped UWB antenna by PSO," *IEEE Antennas Wireless Propag. Lett.*, vol. 6, pp. 182–185, 2007.

[31] E. B. Whiting, S. D. Campbell, G. Mackertich-Sengerdy, and D. H. Werner, "Dielectric resonator antenna geometry-dependent performance tradeoffs," *IEEE Open J. Antennas Propag.*, vol. 2, pp. 14–21, 2021.

[32] L. Lizzi, F. Viani, R. Azaro, and A. Massa, "A PSO-driven spline-based shaping approach for ultrawideband (UWB) antenna synthesis," *IEEE Trans. Ant. Prop.*, vol. 8, pp. 2613–2621, 2008.

[33] J. Bandler, Q. Cheng, and S. Dakroury, "Space mapping: The state of the art," *IEEE Trans. Microw. Theory Techn.*, vol. 52, no. 1, pp. 337–361, Jan. 2004.

[34] A. I. J. Forrester and A. J. Keane, "Recent advances in surrogate-based optimization," *Prog. Aerosp. Sci.*, vol. 45, pp. 50–79, Jan./Apr. 2009.

[35] S. Koziel and A. Bekasiewicz, *Multi-Objective Design of Antennas Using Surrogate Models*. Singapore: World Scientific, 2016.

[36] A. I. Forrester, A. Sobester, and A. J. Keane, "Multi-fidelity optimization via surrogate modeling," *Proc. Roy. Soc.*, vol. 463, pp. 3251–3269, Oct. 2007.

[37] T. W. Simpson, J. Peplinski, P. N. Koch, and J. K. Allen, "Metamodels for computer-based engineering design: Survey and recommendations," *Eng. Comput.*, vol. 17, no. 2, pp. 129–150, Jul. 2001.

[38] S. Koziel and S. Ogurtsov, *Antenna Design by Simulation-Driven Optimization*. New York, NY, USA: Springer, 2014.

[39] S. Koziel and L. Leiffson, *Surrogate-Based Modeling and Optimization*. New York, NY, USA: Springer, 2013.

[40] A. Bekasiewicz, S. Koziel, P. Plotka, and K. Zwolski, "EM-driven multi-objective optimization of a generic monopole antenna by means of a nested trust-region algorithm," *Appl. Sci.*, vol. 11, 2021, Art. no. 3958.

[41] *CST Microwave Studio, Version 2015, Dassault Systems, 10 Rue Marcel Dassault, CS 40501*, Vâlizy-Villacoublay, Cedex, France, 2015.

[42] J. W. Bandler, Q. S. Cheng, N. K. Nikolova, and M. A. Ismail, "Implicit space mapping optimization exploiting preassigned parameters," *IEEE Trans. Microw. Theory Techn.*, vol. 52, no. 1, pp. 378–385, Jan. 2004.

[43] S. Koziel and A. Bekasiewicz, "Implicit space mapping for variable-fidelity EM-driven design of compact circuits," *IEEE Microw. Wireless Comp. Lett.*, vol. 28, pp. 275–277, 2018.

[44] A. Conn, N. I. M. Gould, and P. L. Toint, *Trust-Region Methods* (MPS-SIAM Series on Optimization). Philadelphia, PA, USA: SIAM, 2000.

[45] M. Gupta and V. Mathur, "Wheel shaped modified fractal antenna realization for wireless communications," *AEU-Int. J. Electron. Commun.*, vol. 79, pp. 257–266, Sep. 2017.

[46] T. K. Saha, C. Goodbody, T. Karacolak, and P. K. Sekhar, "A compact monopole antenna for ultra-wideband applications," *Microw. Opt. Technol. Lett.*, vol. 61, pp. 182–186, Oct. 2019.

[47] R. N. Tiwari, P. Singh, and B. K. Kanaujia, "A modified microstrip line fed compact UWB antenna for WiMAX/ISM/WLAN and wireless communications," *AEU-Int. J. Electron. Commun.*, vol. 104, pp. 58–65, May 2019.

[48] A. Poulose and D. S. Han, "UWB indoor localization using deep learning LSTM networks," *Appl. Sci.*, vol. 10, Oct. 2020, Art. no. 6290.

[49] M. Capstick, S. Kuehn, N. Kuster, and N. Kuster, "Measurement technology for electrically small antennas," in *Proc. Loughborough Antennas Propag. Conf. (LAPC)*, Loughborough, U.K., Nov. 2016, pp. 1–5.

[50] B. Yanakiev, J. Nielsen, and G. Pedersen, "On small antenna measurements in a realistic MIMO scenario," in *Proc. Eur. Conf. Ant. Prop.*, Barcelona, Spain, 2010, pp. 1–5.

[51] B. Chen, J. He, Y. Guo, S. Pan, X. Ye, and J. Fan, "Multi-ports (2^n) 2×-thru De-embedding: Theory, validation, and mode conversion characterization," *IEEE Trans. Electromagn. Compatibility*, vol. 61, no. 4, pp. 1261–1270, Aug. 2019.

[52] A. Morales, S. S. Agili, and T. Meklachi, "S-parameter sampling in the frequency domain and its time-domain response," *IEEE Trans. Instr. Meas.*, vol. 70, 2021, Art. no. 6501113.

[53] S. Loredo, M. R. Pino, F. Las-Heras, and T. K. Sarkar, "Echo identification and cancellation techniques for antenna measurement in non-anechoic test sites," *IEEE Antennas Propag. Mag.*, vol. 46, no. 1, pp. 100–107, Feb. 2004.

[54] Y.-T. Hsiao, Y.-Y. Lin, Y. C. Lu, and H.-T. Chou, "Applications of time-gating method to improve the measurement accuracy of antenna radiation inside an anechoic chamber," in *Proc. IEEE Antennas Propag. Soc. Int. Symp.*, vol. 3, Jun. 2003, pp. 794–797.

• • •